2018 IEEE-RAS 18th International Conference on Humanoid Robots (Humanoids)
Beijing, China, November 6-9, 2018

Projected Force-Admittance Control for Compliant Bimanual Tasks

Jianfeng Gao, You Zhou and Tamim Asfour

***Abstract*— Bimanual manipulation is fundamental for humanoid robots. It has gained a lot of attention in robotics research as a key ability towards versatile behavior. To achieve such behaviors in real-world tasks, bimanual controllers must be stable and simple to implement. On the other hand, admittance and impedance control frameworks are well-known for their efficiency in robot's manipulation tasks which require compliant motions e. g. for physical human-robot interactions. Based on these frameworks, we propose a new control framework, the Projected Force-Admittance Control (PFAC), for compliant bimanual manipulation tasks. By analyzing the load distribution in bimanual tasks using grasp mapping technique, the controller uses the projected constraint force, which, together with the actuation force given by the PI controller, are fed into an admittance control framework, and finally provides the virtual target pose to an impedance controller that can be modeled as a mass-spring-damper system. With this control strategy, we ensure motion synchronization and target force regulation under external perturbations and/or while tracking a trajectory. We demonstrate the stability and usability of the controller in several experiments with the humanoids robot ARMAR-6. Combining it with movement primitives approaches such as Dynamic Movement Primitive (DMP), a variety of compliant bimanual tasks are implemented and evaluated.**

I. Introduction and Related Work

Robots have long been expected to work alongside people to provide physical assistance to elderly people or to cooperate with workers, or to do domestic chores. However, environments are designed for human, where a great number of objects need to be manipulated bimanually. The robot needs to perform a precise wrench to the manipulated object to maintain the contact constraints while following a trajectory and dealing with external perturbations. For example, carrying a heavy box and putting it in a specified position. The box could be disturbed by the environment. During interacting with the environment, it is necessary for the robot to take into account the contact force/torque, which enables the compliant control for bimanual tasks and is also important when the object to be manipulated is deformable and a required force is present.

Mechanical impedance was introduced into robotics in [1] where an impedance controller mimics a mass-spring-damper system, which makes it possible to specify a dynamic behavior of a robot arm when physically interacting with the environment. Meanwhile, position-force hybrid control scheme and its variants were proposed in [2] [3], where the task space is decoupled geometrically into position-controlled and force-controlled subspaces. A hybrid impedance control scheme combining the above methods was proposed in [4]. This hybrid scheme requires that the control principle is maintained along every degree of freedom of the arm, which allows task-specific switching between position and force control. However, this approach requires an explicit specification of the control strategy for each degree of freedom, which is only possible in simple environments, but usually impossible for a humanoid robot facing a sophisticated human-robot interaction.

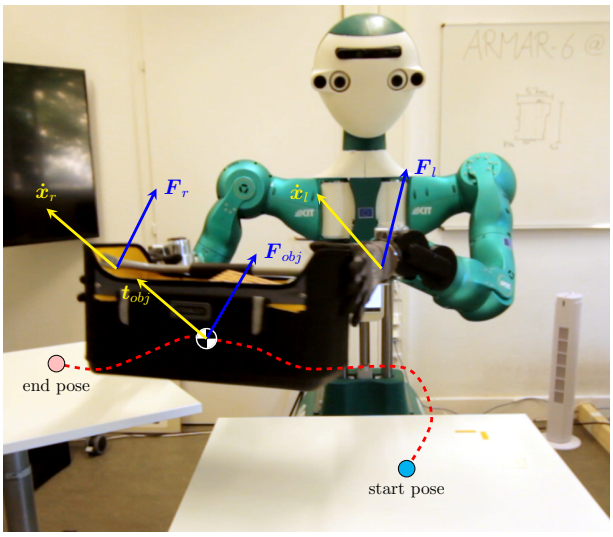

Fig. 1: Bimanual manipulation with the ARMAR-6 robot using PFAC. The robot holds a loaded basket bimanually and executes a trajectory (red dashed line) from start pose (cyan circle) to end pose (pink circle) generated by a movement primitive, subject to some external perturbations $\boldsymbol{F}_{l/r}$.

Bimanual manipulation control by using grasp matrix proposed in the robot grasping literature [5] has a long history [6]. Recent works combine projected inverse dynamic control, which is a state-of-art control framework proposed in [7] and [8], with the grasp matrix idea described in [9] [10], where an optimization algorithm is used instead of explicit force control. However, in this paper, the goal is to design a real-time controller that runs at least 1 kHz, which makes the non-optimization based algorithms a better choice.

Bimanual manipulation control based on the object dynamic model were presented e. g. in [11], [12] and [13], where authors introduce the object dynamic to the con-

The research leading to these results has received funding from the European Union's Horizon 2020 Research and Innovation programme under grant agreement No 643950 (SecondHands) and from the German Research Foundation (DFG: Deutsche Forschungsgemeinschaft) under Priority Program on Autonomous Learning (SPP 1527).

The authors are with the Institute for Anthropomatics and Robotics, Karlsruhe Institute of Technology, Karlsruhe, Germany. urehg@student.kit.edu, {you.zhou, asfour}@kit.edu

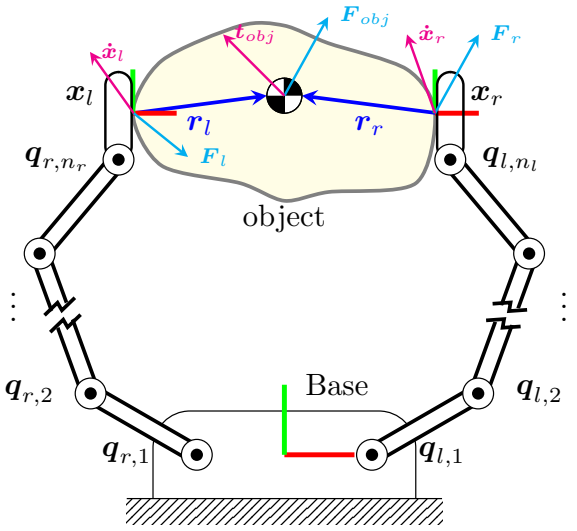

Fig. 2: Model for bimanual manipulation. We assume a fixed robot platform with two arms. In all our experiments (see the attached video), we use the humanoid robot ARMAR-6 without closing hands to form a unilateral contact as shown in this figure.

trollers, together with the dual-arm dynamics, defining an object-level bimanual controller. However, this control strategy has its limitations regarding the unknown object model, which is normally hard to access in practice.

Regarding the unified model combining impedance and admittance control, we refer to [14]. A good review on dual-arm manipulation can be found in [15], [16] and [17].

In this paper, we present a new control framework called Projected Force-Admittance Control (PFAC) to realize a stable compliant bimanual manipulation.

II. Our Approach

We propose a new control framework, the Projected Force-Admittance Control (PFAC), which can be simply considered as an impedance controller with a modified virtual target pose calculated based on both projected force (see Sec. II-A) and force-based PI-controller. The controller guarantees stable compliant bimanual manipulations, the desired contact force, and the real-time control cycle under $400\mu s$.

In the following sections, we describe our approach in details. In Sec. II-A, we analyze the load distribution, so that the hard contact for bimanual grasp cannot be broken and the robot can automatically coordinate both arms under unbalanced perturbations. In Sec. II-B, we derive the extended admittance control based on the projected measured force, the output of a force-based PI-controller. The output of the admittance controller, as a virtual target pose, is consistent with free-motion and internal target force, and is further given to an impedance controller II-C, which outputs final control signals.

A. Projected Force for Bimanual Manipulation

Fig. 2 shows an illustration of a bimanual robot system which we will use to describe our controller. Assume that each arm is fully actuated with n_i DoF, where $i = \{l, r\}$ is the index for the left and right arm, $\boldsymbol{q} = [\boldsymbol{q}_l^T, \boldsymbol{q}_r^T]^T$ is the generalized coordinates, $\boldsymbol{x} = [\boldsymbol{x}_l^T, \boldsymbol{x}_r^T]^T$ is the generalized coordinates for TCP (Tool Center Point) frames of the two hands expressed in the base frame, and $\boldsymbol{F}_x = [\boldsymbol{F}_{x,l}^T, \boldsymbol{F}_{x,r}^T]^T \in \mathbb{R}^{12}$ is the external force applied to the end-effectors of the robot expressed in the base frame. (Note that, in the rest of this paper, if not specified, the position, velocity, acceleration and force vectors are all expressed in the base frame, and for simplicity we eliminate the superscript. For example, ${}^B\boldsymbol{x}$ is simplified to $\boldsymbol{x}$).

As defined in [5], the grasp matrix for dual-arm system can be expressed as

$$\boldsymbol{G} = \begin{bmatrix} \boldsymbol{G}_l & \boldsymbol{G}_r \end{bmatrix} = \begin{bmatrix} \boldsymbol{I}_3 & \boldsymbol{0}_3 & \boldsymbol{I}_3 & \boldsymbol{0}_3 \\ \boldsymbol{S}(\boldsymbol{r}_l)^T & \boldsymbol{I}_3 & \boldsymbol{S}(\boldsymbol{r}_r)^T & \boldsymbol{I}_3 \end{bmatrix}, \quad (1)$$

where $\boldsymbol{I}_3, \boldsymbol{0}_3$ are 3-dimensional identity matrix and zero matrix, $\boldsymbol{S}(\cdot)$ is the skew-symmetric operator and $\boldsymbol{r}_l, \boldsymbol{r}_r$ are the position vectors from left and right end-effector to an arbitrary point of the manipulated object, as shown in Fig. 2. It can be easily derived from rigid body dynamics that the following constraint equations hold,

$$\dot{\boldsymbol{x}} = \boldsymbol{J}\dot{\boldsymbol{q}} = \boldsymbol{G}^T\boldsymbol{t}_{obj} \quad (2a)$$

$$\boldsymbol{F}_{obj} = \boldsymbol{G}\boldsymbol{F}_x, \quad (2b)$$

where $\boldsymbol{t}_{obj}, \boldsymbol{F}_{obj} \in \mathbb{R}^6$ are twist (linear and angular velocity) and generalized force (force and torque) of the object respectively, and 2a and 2b are the velocity and force constraints for grasp with hard contact respectively.

Any force vector can be decomposed as

$$\boldsymbol{F}_x = \boldsymbol{F}_{unc} + \boldsymbol{F}_c = \boldsymbol{G}^\dagger\boldsymbol{G}\boldsymbol{F}_x + \boldsymbol{P}_G\boldsymbol{F}_x \quad (3)$$

where $\boldsymbol{P}_G = (\boldsymbol{I}_{12} - \boldsymbol{G}^\dagger\boldsymbol{G})$ is the null-space projection and $\boldsymbol{G}^\dagger$ is the pseudo-inverse of grasp matrix. The term $\boldsymbol{F}_{unc}$ represents the unconstrained force (also called the external force in some literature), which induces free-motion, while the second term $\boldsymbol{F}_c$ is the constrained force (also called internal force), which does not produce any motion. However, the unconstrained force cannot be directly used for admittance control on a torque controlled robot with impedance behaviors, since the above analysis is valid only if the hard constraints for bimanual manipulation are not violated. However violation of the contact constraints could happen when tangential frictions are small, or the contact surface is not big enough, which is especially the case for unilateral contact and bimanually grasping of a board with thin edges or slippery round object.

To address this problem, we analyze the steady-state admittance behavior of a torque controlled dual-arm robot with an example. Although this is a special case, the result can be used in any other scenario. As depicted in Fig. 3a, the two hands are unilaterally in contact with a round-sided object with a low friction surface, and some external force $F_{x,ly}$ is only applied to the left hand along the y-axis, and the target force vectors are $F_{d,lx}, F_{d,rx}$ along x-axis. Now consider the motion induced along y axis and start

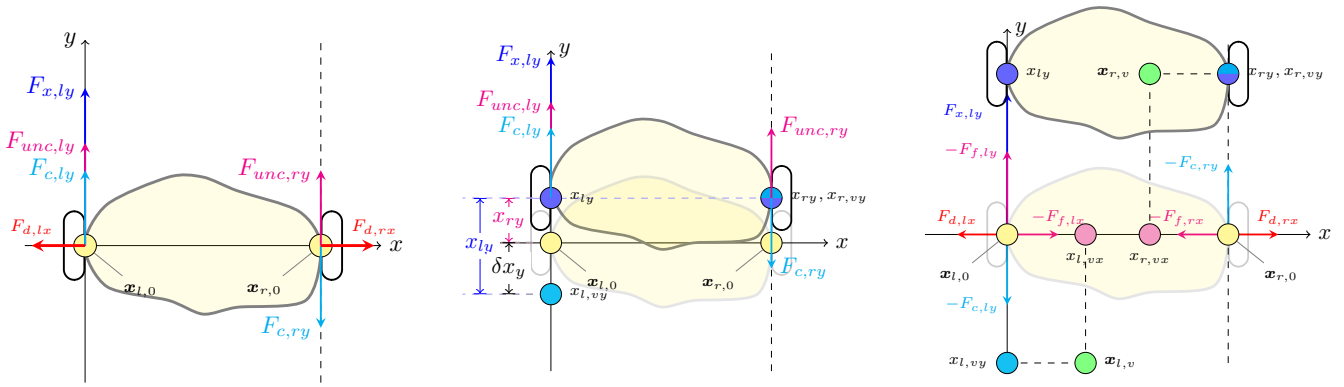

(a) force projection

(b) asynchronous motion

(c) virtual pose computed from extended admittance control

Fig. 3: Force projection for motion synchronization using extended admittance control. **Left:** an external perturbation $F_{x,ly}$ is applied on left hand and projected to constraint $F_{c,ly/ry}$ and unconstrained $F_{unc,ly/ry}$ forces. **Middle:** the expected synchronous motion in y axis can be guaranteed by pose modification, which is controlled by $\delta x_y = x_{ry} - x_{ly}$. The initial, modified and final steady-state pose are represented in yellow, cyan and blue circles respectively. **Right:** the extended admittance control sets the virtual target poses (see green circles) for impedance control, whose components in the direction perpendicular to the target force (here, y-axis) are calculated based on negated constraint force and force-based PI-controller (see cyan circles) and components in the direction of the target force (here, x-axis) is given by only force-based PI-controller (see pink circles). Finally, blue circles are steady states for both arms after control.

from the original pose $\boldsymbol{x}_{l,0}, \boldsymbol{x}_{r,0}$. Since the arms possess impedance behavior, the left arm moves a distance induced from $F_{x,ly}$ bigger than the expected distance induced from $F_{unc,ry}$, which leads to the violation of the constraints and asynchronous motion of the two hands. While the expected synchronous motion along y axis is shown in Fig. 3b. As long as the synchronous motion is guaranteed, the grasp constraint is valid. Notice that $F_{unc,ly/ry}$ are the target forces to induce free-motion that is consistent with the grasp constraint, while the actual force applied is $F_{x,ly}$. Since the system is modeled as a spring in the steady state, the position of "the end point of the spring" can be controlled by modifying "the start point of the spring". So, to achieve synchronous motion along y axis we need to move the initial pose of the left arm backward and that of the right arm forward. The amount of modification for the left arm satisfies

$$\delta x_y = K_p^{-1}(F_{unc,ly} - F_{x,ly}) = -K_p^{-1}F_{c,ly}, \tag{4}$$

where K_p is the stiffness coefficient of impedance controller in this direction. This mechanism shows that we can use the constrained force to modify the virtual contact poses for the impedance controllers of both arms.

Based on this idea, we propose a novel method in II-B, which ensures the synchronous motion of two hands while precisely applying a desired force to the object without violation of the unilateral contact constraints.

B. The Extended Admittance Control for Virtual Contact

In the real world, the noise in the force feedback leads to a very jittery pose modification. An admittance control framework, which models the system as a mass-spring-damper system, is used as the pose modifier to produce smooth pose modification induced from some general force, which consists of the feedback force and/or the computed actuation force.

The task space admittance model is expressed as

$$\boldsymbol{H}\ddot{\tilde{\boldsymbol{x}}} + \boldsymbol{D}\dot{\tilde{\boldsymbol{x}}} + \boldsymbol{K}\tilde{\boldsymbol{x}} = \boldsymbol{F}, \tag{5}$$

where $\boldsymbol{H}, \boldsymbol{D}, \boldsymbol{K}$ are desired task space inertial matrix, damping matrix and stiffness matrix respectively, $\boldsymbol{F}$ is the generalized force applied to the dynamic system and $\tilde{\boldsymbol{x}} = \boldsymbol{x}_v - \boldsymbol{x}_0$ is the pose difference between the virtual pose $\boldsymbol{x}_v$ and the initial pose $\boldsymbol{x}_0$.

Fig. 3 shows the whole concept of the extended admittance control. The internal force represents the "squeezing force" to the object. Considering a desired force vector $\boldsymbol{F}_d \in \mathbb{R}^{12}$ and taking the measured force $\boldsymbol{F}_x$ as feedback, we can create a simple PI-controller to track the target force trajectory. Since the I-term does not vanish after a duration of external perturbation, the I-term produces free motions and drives the robot away from the original trajectory. In order to avoid this when following a desired trajectory is of higher priority, we multiply the I-term by a decay coefficient $e^{-\eta t}$ so that we can control the velocity of the hand to return to a specified trajectory after perturbation with $\eta > 0$. In some special task, we might prefer a not decayed I-term by setting $\eta = 0$. The actuation force for internal target force regulation $\boldsymbol{F}_f$ can be computed as

$$\boldsymbol{F}_f = \boldsymbol{K}_{P,f}\boldsymbol{e}_f + e^{-\eta t}(\boldsymbol{K}_{I,f}\int_{t_0}^{t_e}\boldsymbol{e}_f dt). \tag{6}$$

where $\boldsymbol{K}_{P,f}, \boldsymbol{K}_{I,f}$ are PI feedback gains, and $\boldsymbol{e}_f = \boldsymbol{F}_d - \boldsymbol{F}_c$ is the force error.

To achieve synchronous motion and regulation of target force, the generalized force $\boldsymbol{F}$ for admittance control requires the contribution from both the projected feedback force $\boldsymbol{F}_c$

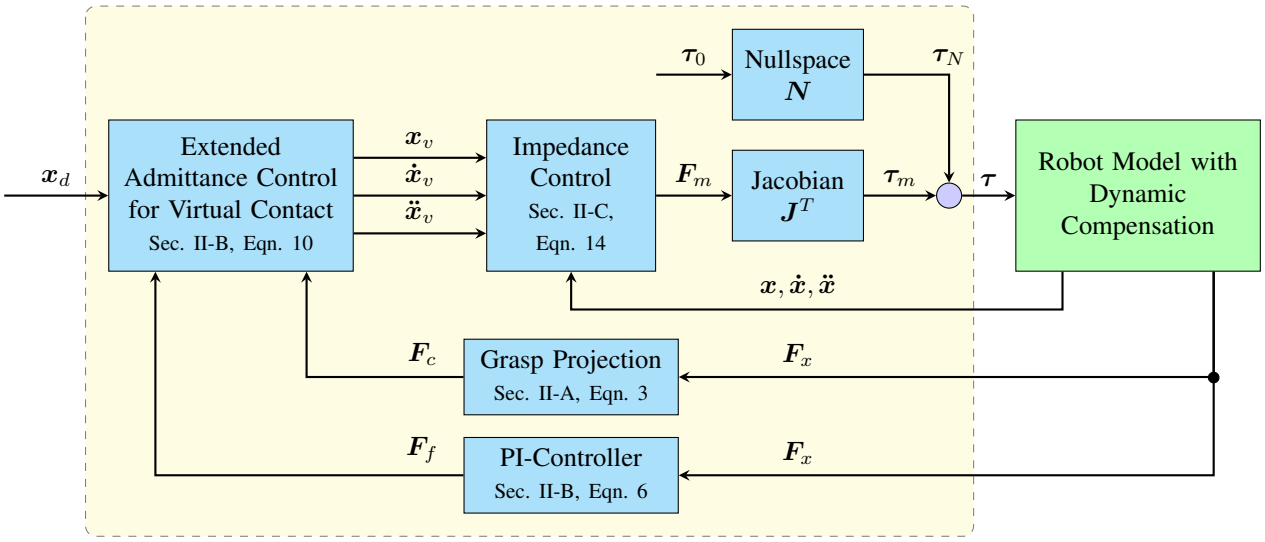

Fig. 4: Projected Force-Admittance Controller Diagram. The yellow region shows our control framwork, which takes the desired pose $\boldsymbol{x}_d$ from movement primitives such as DMP ([18], [19]), the current state vectors $\boldsymbol{x}, \dot{\boldsymbol{x}}, \ddot{\boldsymbol{x}}$ and measured force $\boldsymbol{F}_x$ as inputs and outputs the target torque signal.

and the actuation force $\boldsymbol{F}_f$ computed from the PI force controller, $\boldsymbol{F} = -(\alpha \boldsymbol{F}_f + \beta \boldsymbol{F}_c)$. The resolved acceleration of the virtual state can be computed by inserting the combination of the two forces into the admittance control scheme,

$$\ddot{\boldsymbol{x}}_v = \ddot{\boldsymbol{x}}_d - \boldsymbol{K}_{d,A}\dot{\tilde{\boldsymbol{x}}} - \boldsymbol{K}_{p,A}\tilde{\boldsymbol{x}} - \boldsymbol{K}_{m,A}(\alpha \boldsymbol{F}_f + \beta \boldsymbol{F}_c), \quad (7)$$

where $\boldsymbol{K}_{d,A} = \boldsymbol{H}^{-1}\boldsymbol{D}, \boldsymbol{K}_{p,A} = \boldsymbol{H}^{-1}\boldsymbol{K}, \boldsymbol{K}_{m,A} = \boldsymbol{H}^{-1}$ and $\alpha, \beta \in \mathbb{R}$ are coefficients of linear combination of $\boldsymbol{F}_f$ and $\boldsymbol{F}_c$. Finally, the virtual state can be integrated from the resolved acceleration, e.g. using Netwon-Euler method. Therefor the virtual state $\boldsymbol{x}_v$ is consistent with the synchronous motion and the regulation of target force. The virtual pose $\boldsymbol{x}_v = [\boldsymbol{x}_{v,l}^T, \boldsymbol{x}_{v,r}^T]^T$ indicates the desired grasping pose of the two hands.

The modification of the virtual state depends on the impedance/admittance stiffness matrix $\boldsymbol{K}_p, \boldsymbol{K}_{p,A}$, the admittance initial matrix $\boldsymbol{H}$ and the coefficient α, β. The certain relationship of these parameters guarantees that the synchronous motion under external perturbations can be achieved. Fig. 3c shows the new steady-state behavior with synchronous and constraint consistent motion under the perturbation $\boldsymbol{F}_{x,ly}$. In the tangential space of target force $\boldsymbol{F}_d$, motion synchronization requires that $(x_{ly} - x_{l,0y}) = (x_{ry} - x_{r,0y})$, thus $(x_{ly} - x_{l,vy}) + (x_{l,vy} - x_{l,0y}) = (x_{r,vy} - x_{r,0y})$. In the steady-state, we have

$$\frac{F_{x,ly}}{K_p} - \frac{\beta K_{m,A} F_{c,ly} + \alpha K_{m,A} F_{f,ly}}{K_{p,A}} = \frac{-\beta K_{m,A} F_{c,ry}}{K_{p,A}} \quad (8)$$

where $F_{f,ly} = K_{P,f}(0 - F_{x,ly}) = -K_{P,f} F_{x,ly}$, since the target force in y direction is zero. And $F_{c,ly} = -F_{c,ry} = \gamma F_{x,ly}$, where $\gamma \in \mathbb{R}$ is a constant determined by grasp matrix. Extend to more general case, the controller parameters satisfy

$$\boldsymbol{K}_{p,A} = (2\beta\gamma \boldsymbol{I} - \alpha \boldsymbol{K}_{P,f}) \boldsymbol{K}_{m,A} \boldsymbol{K}_p, \quad (9)$$

which shows when impedance/admittance behaviors are specified, there is a trade-off of the amount of modification of the virtual poses induced by projected feedback force $\boldsymbol{F}_c$ and the actuation force $\boldsymbol{F}_f$, which can be balanced by modifying α and β. To avoid $\boldsymbol{F}_c$ and $\boldsymbol{F}_f$ interfering with each other for internal force regulation, the vector resolution of $\boldsymbol{F}_c$ in the direction of $\boldsymbol{F}_d$, denoted as $\boldsymbol{F}_c^r$, is eliminated.

To this end, the desired virtual target pose to be used in impedance controller (derived in section II-C) can be computed by integrating the following resolved virtual acceleration

$$\ddot{\boldsymbol{x}}_v = \ddot{\boldsymbol{x}}_d - \boldsymbol{K}_{d,A}\dot{\tilde{\boldsymbol{x}}} - \boldsymbol{K}_{p,A}\tilde{\boldsymbol{x}} - \boldsymbol{K}_{m,A}(\alpha \boldsymbol{F}_f + \beta(\boldsymbol{F}_c - \boldsymbol{F}_c^r)), \quad (10)$$

C. Impedance Control for Virtual Pose Grasping

The task space dynamic equation of the dual-arm robot can be expressed as

$$\boldsymbol{\Lambda}\ddot{\boldsymbol{x}} + \boldsymbol{\Lambda}(\boldsymbol{J}\boldsymbol{M}^{-1}\boldsymbol{h} - \dot{\boldsymbol{J}}\dot{\boldsymbol{q}}) = \boldsymbol{\Lambda}\ddot{\boldsymbol{x}} + \boldsymbol{h}_c = \boldsymbol{F}_m + \boldsymbol{F}_x, \quad (11)$$

where $\boldsymbol{M} = \text{blockdiag}\ \{\boldsymbol{M}_l, \boldsymbol{M}_r\}, \boldsymbol{J} = \text{blockdiag}\ \{\boldsymbol{J}_l, \boldsymbol{J}_r\}$ are the inertia matrix and the Jacobian matrix of the system, $\boldsymbol{h}$ includes the centrifugal, Coriolis force, the friction force and the gravitational force, and $\boldsymbol{\tau}_m = [\boldsymbol{\tau}_l^T, \boldsymbol{\tau}_r^T]^T$ is the actuation torque vector for all joints. where $\boldsymbol{\Lambda} = (\boldsymbol{J}\boldsymbol{M}^{-1}\boldsymbol{J}^T)^{-1}$ is the task space inertia matrix, $\boldsymbol{\tau}_m = \boldsymbol{J}^T\boldsymbol{F}_m$, with $\boldsymbol{F}_m$ the equivalent actuation force expressed in task space, and $\boldsymbol{h}_c$ the task space Coriolis force, friction and gravitational force.

A typical task space mechanical impedance can be modeled as mass-spring-damper system,

$$\boldsymbol{K}_m\ddot{\tilde{\boldsymbol{x}}} + \boldsymbol{K}_d\dot{\tilde{\boldsymbol{x}}} + \boldsymbol{K}_p\tilde{\boldsymbol{x}} = \boldsymbol{F}_x \quad (12)$$

$$\ddot{\boldsymbol{x}} = \boldsymbol{K}_m^{-1}(\boldsymbol{K}_m\ddot{\boldsymbol{x}}_v - \boldsymbol{K}_d\dot{\tilde{\boldsymbol{x}}} - \boldsymbol{K}_p\tilde{\boldsymbol{x}} + \boldsymbol{F}_x), \quad (13)$$

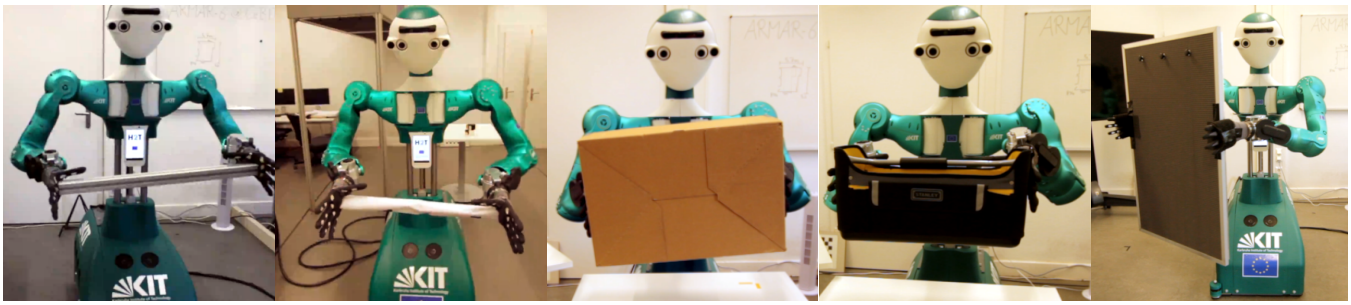

(a) Aluminum Beam (b) Paper Roll (c) Box (d) Basket (e) Large Board

Fig. 5: ARMAR-6 robot uses PFAC for bimanual tasks. 5 different types of objects are used in our experiments to evaluate the performance of the controller. For each object, the controller is tested while maintaining a static pose (Sec. III-B) and tracking a trajectory (Sec. III-C)

where $\tilde{\boldsymbol{x}} = \boldsymbol{x} - \boldsymbol{x}_v$ is the pose error between current pose $\boldsymbol{x}$ and virtual target pose $\boldsymbol{x}_v$. The coefficient matrix $\boldsymbol{K}_m, \boldsymbol{K}_d, \boldsymbol{K}_p$ represent the desired task space inertia matrix, damping factors and stiffness factors respectively. With the virtual target pose vector computed from II-B, the actuation force for motion $\boldsymbol{F}_m$ can be computed by substituting 13 into 11 and considering the desired task space inertia matrix equivalent to the inertia matrix of the robot $\boldsymbol{K}_m = \boldsymbol{\Lambda}$,

$$\boldsymbol{F}_m = \boldsymbol{\Lambda}\ddot{\boldsymbol{x}}_v - \boldsymbol{K}_d\dot{\tilde{\boldsymbol{x}}} - \boldsymbol{K}_p\tilde{\boldsymbol{x}} + \boldsymbol{h}_c \tag{14}$$

For a torque-controlled robot, we can easily map the task space actuation force to joint space, and a null-space control strategy is used to specify some joint nullspace behaviors,

$$\boldsymbol{\tau} = \boldsymbol{\tau}_m + \boldsymbol{\tau}_N = \boldsymbol{J}^T\boldsymbol{F}_m + \boldsymbol{N}\boldsymbol{\tau}_0, \tag{15}$$

where $\boldsymbol{N} = (\boldsymbol{I}_n - \boldsymbol{J}^T\boldsymbol{J}^{T\dagger})$ is the null-space projector, and $\boldsymbol{\tau}_0$ is an arbitrary n-dimensional vector, where $n = n_l + n_r$. For example, a typical choice is $\boldsymbol{\tau}_0 = \boldsymbol{K}_{p,N}\boldsymbol{e}_q + \boldsymbol{K}_{d,N}\dot{\boldsymbol{e}}_q$, where $\boldsymbol{K}_{p,N}, \boldsymbol{K}_{d,N}$ are PD gains and $\boldsymbol{e}_q = \boldsymbol{q}_d - \boldsymbol{q}$, where $\boldsymbol{q}$ is the actual joint values and $\boldsymbol{q}_d$ is the desired joint values, which can be learned from demonstration.

An overview of Projected Force-Admittance Controller (PFAC) is shown in Fig. 4.

III. Experimental Evaluation

A. Experimental Setup

The controllers are implemented in ArmarX[1] and the experiments are conducted on the ARMAR-6 humanoid robot [20], which comprises 2 torque-controlled arms with 8-DoF each and 2 ATI force-torque sensors in the wrists. The force feedback data is filtered through IIR filters and moving mean filters. All the joints of the dual-arm are torque controlled and a low-level zero-torque controller ensures that the robot arms hold its pose without external force. Parameters are designed by first specifying a desired impedance behavior for a specific task and then tuning the PI parameters, the admittance parameters and the balancing coefficients according to (9).

[1]https://armarx.humanoids.kit.edu

Experiments are divided into two parts to show the stability and usability of PFAC. 1) Motion synchronization and target force regulation at a static target pose. Human perturbations are applied to the hands or the objects. 2) Tracking a trajectory, generated by DMP ([18] [19]), subject to arbitrary perturbations.

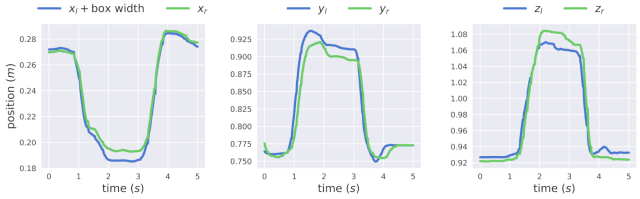

Fig. 6: Motion synchronization under single perturbation at static pose while holding the box. Since the x positions of the two hands are symmetric about the $y-z$ plane with a distance of box width, we add the box width to x_l to show the synchronous motion more clearly.

B. Bimanual Manipulation at Static Pose

In this set of experiments, the robot holds different types of the object respectively with our controller at the static pose and we apply some external force in an arbitrary direction, then we evaluate the motion synchronization and the regulation of the target force on the object. We choose a $80cm$ of 4545 aluminum beam, a paper roll, a box ($60 \times 40 \times 20cm$), a basket ($56 \times 28 \times 24cm$) and a large boards ($120 \times 80cm$). The holding pose are showed in Fig. 5.

Firstly, perturbations are applied to on hand in x, y, z axis respectively (see the attached video), and results (see Fig. 6) show that the controller can respond very fast and synchronize both hands quite well (under $1cm$ error). When the external force vanishes, both arm return with the same speed to their original pose. Then we apply a series of external perturbations on the two hands(see Fig. 5a). Since an arbitrary disturbance is applied approximately along the axis in the above sequence, besides the major component on that axis, there are components on other axes. From the first 3 rows of Fig. 7, we can see the good performance of

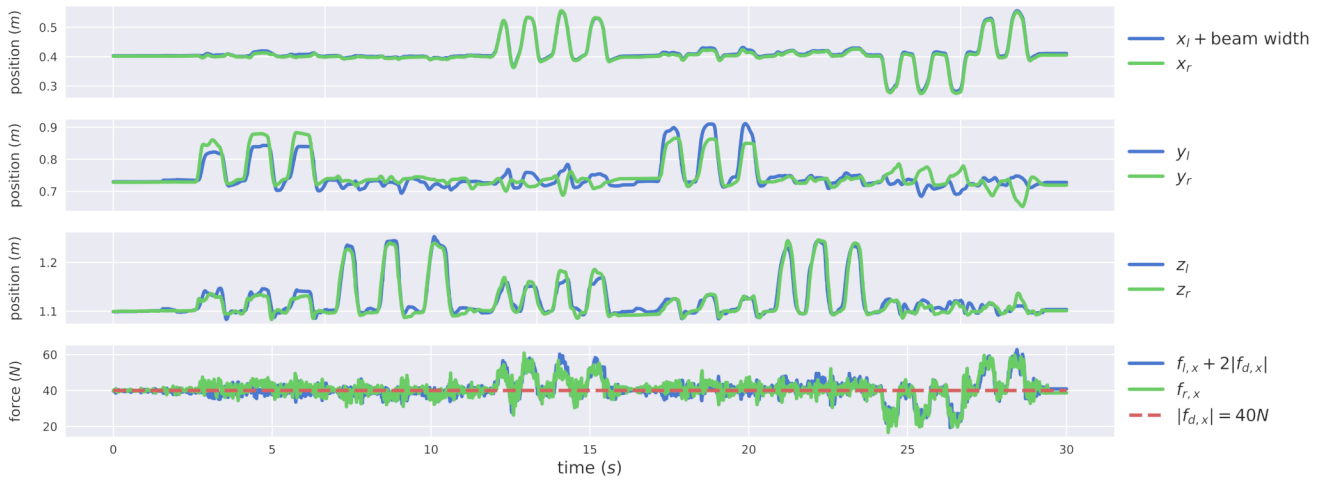

Fig. 7: Synchronous motion and target force evaluation at static pose under a series of perturbations while holding the aluminum beam, with the applying sequence $\{y_l, z_l, x_l, y_r, z_r, x_r\}$, where x_l indicates force applied along the x axis of the left hand. The first 3 rows are the positions of two hands in x, y, z axis respectively and the last row shows the internal force along the x axis, on which the robot apply force to the object. The magnitude of the target force is set to $|f_{d,x}| = 40N$ (dashed line). We add $2|f_{d,x}|$ to the force measurement on the left hand so that the force measurements of the two hands are aligned and thus the synchronous change of the force is more clear.

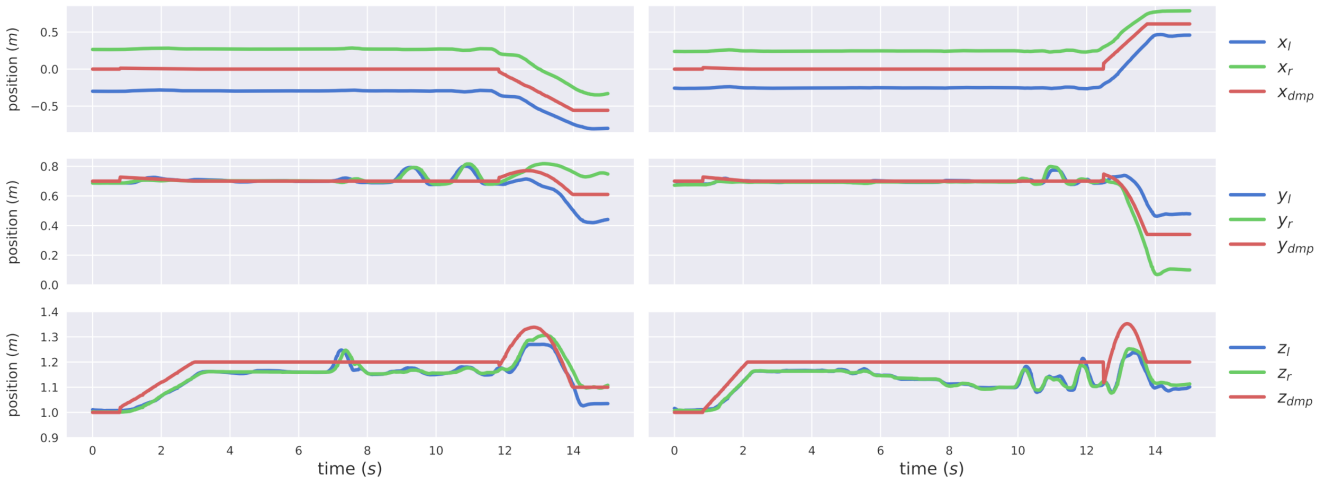

Fig. 8: synchronous motion and target force evaluation when following a trajectory. **Left**: diagrams show the experiment of moving the empty basket to the left side of the robot; **Right**: diagrams show the experiment of dynamically loading the basket and then move to the right side of the robot. Three rows show positions in x, y, z axis separately. The trajectory of the center of the basket is given by DMP which is learned from demonstrations.

motion synchronization. The last row shows the target force regulation. When no external perturbation occurs, the internal force is regulated around the target force with a very small range of oscillation, this can be shown at first few seconds of the plotting. The perturbation on x-axis has a great influence on the internal force regulation, but the regulation comes back as soon as the external force vanishes. The perturbation on the other direction has little influence. Experiments with other objects show the same result.

C. Bimanual Manipulation with Movement

In this set of experiments, the robot transports different objects with learned Dynamic Movement Primitive (DMP) from demonstrations. In this experiments, DMP outputs the next desired pose of the box. However, nothing avoids that DMP outputs directly the desired target pose of the hands, which can form a coherent control system based on our controller.

Fig. 8 shows the tracking of the trajectory generated by DMP and the target force regulation while carrying

the basket (see Fig. 5d). The first two rows show a good performance of tracking in x, y axis, even under unexpected perturbation. For the third row that shows the tracking performance in z axis, there is a constant distance between DMP output and the trajectory of the hands in the left picture, and a time-varying distance in the right one. The constant distance is induced by the constant gravity force of the basket, while the time-varying part in the right picture indicates the dynamically loading process. The fully loaded basket is about $6kg$.

Experiments for moving other objects mentioned above using the same trajectory show the same result. The heavier the object is, the larger distance in z axis presents. Although, the performance resisting the external perturbation shows stability and robustness in any conditions.

IV. Conclusions and Future Works

In this paper, we propose the Projected Force-Admittance Control framework, which modifies the virtual pose induced from the constrained force and the actuation force computed from a PI-controller, by properly setting of the controller parameters and analyzing the load distribution. The experiments of the ARMAR-6 robot holding different objects with different shapes and weights under arbitrary human interactions show the stability and robustness of our controller when targeted at a static pose. Further experiments of the robot following a trajectory generated by DMP demonstrate the stability under dynamic bimanual tasks.

However, our present work is limited to hard contact with a rigid object. The grasping map does not dynamically adapt to a deformable object, and thus the contact constraint could be violated. The varying weight of the object is only considered as an external perturbation. In the future, we plan to develop machine learning algorithms for online model estimation to learn grasping map for handling deformable objects and objects with time-varying weights. Besides, we focus on the behavior after impacting with the manipulated object and leave the impact phase (see [21]) as future work, since this is related to manipulating of objects with different stiffness. Currently, we specify a constant target force to examine the regulation behavior of the internal force. This target force trajectory could be learned from demonstration for some specific tasks, so that the internal force vector stays inside the friction cone, as explained in this paper [22].

Furthermore, it is also important for a robot to learn more complex tasks and to choose the most energetically economical path. Quantitative evaluation and fine tuning of the parameters and benchmark of the effect of each parameter on the controller will be conducted in the future to improve the performance of the robot and the battery life.

References

[1] N. Hogan, "Impedance control: An approach to manipulation," in *American Control Conference, 1984*. IEEE, 1984, pp. 304–313.

[2] M. H. Raibert and J. J. Craig, "Hybrid Position/Force Control of Manipulators," *Journal of Dynamic Systems, Measurement, and Control*, vol. 103, no. 2, p. 126, 1981.

[3] M. T. Mason, "Compliance and force control for computer-controlled manipulators," *IEEE Trans on Systems, Man, and Cybernetics*, vol. 11, no. 6, pp. 418–432, January 1981.

[4] R. J. Anderson and M. W. Spong, "Hybrid impedance control of robotic manipulators." *IEEE journal of robotics and automation*, vol. 4, no. 5, pp. 549–556, 1988.

[5] R. M. Murray, Z. Li, and S. S. Sastry, *A Mathematical Introduction to Robotic Manipulation*, 1994, vol. 29.

[6] I. D. Walker, R. A. Freeman, and S. I. Marcus, "Analysis of Motion and Internal Loading of Objects Grasped by Multiple Cooperating Manipulators," *The International Journal of Robotics Research*, vol. 10, no. 4, pp. 396–409, 1991.

[7] F. Aghili, "A unified approach for inverse and direct dynamics of constrained multibody systems based on linear projection operator: Applications to control and simulation," *IEEE Transactions on Robotics*, vol. 21, no. 5, pp. 834–849, 2005.

[8] F. Aghili and C. Y. Su, "Control of constrained robots subject to unilateral contacts and friction cone constraints," *Proceedings - IEEE International Conference on Robotics and Automation*, vol. 2016-June, pp. 2347–2352, 2016.

[9] H.-C. Lin, J. Smith, K. Kouhkiloui Babarahmati, N. Dehio, and M. Mistry, "A Projected Inverse Dynamics Approach for Multi-arm Cartesian Impedance Control," in *IEEE/RSJ Int. Conf. on Robotics and Automation*, 2018.

[10] N. Dehio, J. Smith, D. L. Wigand, G. Xin, H.-C. Lin, J. J. Steil, and M. Mistry, "Modeling and control of multi-arm and multi-leg robots: Compensating for object dynamics during grasping," in *2018 IEEE International Conference on Robotics and Automation (ICRA)*. IEEE, 2018, pp. 294–301.

[11] T. Wimböck, C. Ott, and G. Hirzinger, "Impedance behaviors for two-handed manipulation: Design and experiments," *Proceedings - IEEE International Conference on Robotics and Automation*, no. April, pp. 4182–4189, 2007.

[12] T. Wimböck, C. Ott, A. Albu-Schäffer, and G. Hirzinger, "Comparison of object-level grasp controllers for dynamic dexterous manipulation," *International Journal of Robotics Research*, 2012.

[13] M. Shahbazi, J. Lee, D. Caldwell, and N. Tsagarakis, "Inverse dynamics control of bimanual object manipulation using orthogonal decomposition: An analytic approach," *IEEE International Conference on Intelligent Robots and Systems*, October 2017.

[14] C. Ott, R. Mukherjee, and Y. Nakamura, "A Hybrid System Framework for Unified Impedance and Admittance Control," *J Intell Robot Syst*, vol. 78, pp. 359–375, 2015.

[15] C. Smith, Y. Karayiannidis, L. Nalpantidis, X. Gratal, P. Qi, D. V. Dimarogonas, and D. Kragic, "Dual arm manipulation - A survey," *Robotics and Autonomous Systems*, vol. 60, no. 10, pp. 1340–1353, 2012.

[16] S. Sina Mirrazavi Salehian, N. Figueroa, and A. Billard, "Coordinated multi-arm motion planning: Reaching for moving objects in the face of uncertainty," *Robotics: Science and Systems XII*, 2016.

[17] J. Lee, P. H. Chang, and R. S. Jamisola, "Relative impedance control for dual-arm robots performing asymmetric bimanual tasks," *IEEE Transactions on Industrial Electronics*, vol. 61, no. 7, pp. 3786–3796, 2014.

[18] S. Schaal, "Dynamic movement primitives - a framework for motor control in humans and humanoid robots," in *The International Symposium on Adaptive Motion of Animals and Machines*, 2003.

[19] A. J. Ijspeert, J. Nakanishi, H. Hoffmann, P. Pastor, and S. Schaal, "Dynamical movement primitives: Learning attractor models for motor behaviors," *Neural Comput.*, vol. 25, no. 2, pp. 328–373, Feb. 2013.

[20] T. Asfour, L. Kaul, M. Wachter, S. Ottenhaus, P. Weiner, S. Rader, R. Grimm, Y. Zhou, M. Grotz, F. Paus, D. Shingarey, and H. Haubert, "Armar-6: A collaborative humanoid robot for industrial applications," in *IEEE/RAS International Conference on Humanoid Robots (Humanoids)*, 2018.

[21] T.-J. Tarn, Y. Wu, N. Xi, and A. Isidori, "Force regulation and contact transition control," *IEEE Control Systems*, vol. 16, no. 1, pp. 32–40, 1996.

[22] D. E. Stewart and J. C. Trinkle, "An implicit time-stepping scheme for rigid body dynamics with inelastic collisions and coulomb friction," *International Journal for Numerical Methods in Engineering*, vol. 39, no. 15, pp. 2673–2691, 1996.